Journal of Materials Chemistry

Cite this: *J. Mater. Chem.*, 2011, **21**, 9406

www.rsc.org/materials

HIGHLIGHT

TiO_2 nanotubes: Structure optimization for solar cells

Junfeng Yan[ab] and Feng Zhou*[a]

DOI: 10.1039/c1jm10274e

This review starts with a brief introduction to TiO_2 nanotubes (NTs), and then discusses in more detail how to optimize the structure of TiO_2 NTs for the fabrication of highly efficient solar cells, including the controllable fabrication of perfectly aligned TiO_2 NTs, optimizing the tube parameters, strategies of sensitization, improvement of the interface adhesion in polymer/TiO_2 solar cells and how to make devices flexible. Some key challenges and perspectives for future research are also tentatively discussed.

1. Introduction

Looking for alternative resources is currently a hot research topic world wide in academic society. Among all potential technologies, photovoltaic solar cells have been highly valued,[1–13] new photoelectric conversion materials and device configurations are continuously invented and world-record efficiencies are broken time and time again.[14–19] Besides silicon, anatase TiO_2 is another core inorganic material that is also capable of efficiently harvesting light and is considered the prominent cathode electrode material in solar cells.[20–22] Among different shapes of titania, TiO_2 nanotubes have raised a lot of interest in the last decade. This review outlines recent advances in TiO_2 nanotube based solar cells including polymer solar cells and dye-sensitized solar cells (DSSCs). There have been several reviews on TiO_2 nanotubes,[23–27] and the present one aims to present some novel opinions based on our recent achievements and the latest progress.

TiO_2 is a typical transition metal oxide semiconductor with high chemical stability, low-costs, non-toxicity, strong photocatalytic activity and high photoelectric conversion efficiency. These unique physical and chemical properties render it excellent material for solar energy conversion[2] in dye-sensitized solar cells,[28–31] heterojunction solar cells,[32,33] photocatalysis,[34–39] and many other applications.[40–46] The most widely used photoelectrode in DSSCs is porous TiO_2 films made from nanocrystalline TiO_2 particles which are deposited on conductive glass substrates. In general, the dynamic competition between the

[a]*State Key Laboratory of Solid Lubrication, Lanzhou Institute of Chemical Physics, Chinese Academy of Sciences, Lanzhou, 730000, China. E-mail: zhouf@lzb.ac.cn*
[b]*Graduate School, Chinese Academy of Sciences, Beijing, 100039, China*

Junfeng Yan

Mr Junfeng Yan is currently a Ph.D. student in Lanzhou Institute of Chemical Physics (LICP), Chinese Academy of Sciences. He received his B.Sc. degree in chemistry from Northwest Normal University, China in 2008. In 2008, he joined Prof. Feng Zhou's group at LICP. His current scientific interests focus on the preparation of TiO_2 nanomaterials, particularly anodized TiO_2 nanotubes and their applications in solar cells.

Feng Zhou

Dr Feng Zhou is a Professor in State Key Lab of Solid Lubrication, Lanzhou Institute of Chemical Physics under the "Top Hundred Talents" Program of Chinese Academy of Sciences. He got his PhD in 2004 in the Lanzhou Institute of Chemical Physics. He spent three years (2005–2008) in the Department of Chemistry, University of Cambridge as a postdoctoral research associate. He has published more than 70 journal papers. His research interests are materials interfaces for solar cells and energy storage, the micro/nanostructured surfaces for lubrication, drag/noise reduction and anti-biofouling applications.

electron flow in TiO_2 and the interfacial charge recombination is the key factor to limit the solar cells efficiency. However, in nanoparticle systems, due to the defects, innumerous trapping sites, long travel distance, and disordered contact areas between two TiO_2 nanoparticles, the electron transporting time in the TiO_2 bulk phase is rather long, resulting in more charge recombination and enhanced scattering of free electrons with reduced mobility,[28] thereby reducing the electron collection at the back contact and hence the overall efficiency. Using nanotubular TiO_2 aims to enhance the electron transporting and charge separation efficiency by creating direct pathways for accelerating the charge transfer between interfaces.[47–49]

In comparison with other forms of nanostructured TiO_2 materials, one-dimensional nanomaterials such as nanotubes, especially electrochemical anodized TiO_2 nanotubes, are the most attractive candidates for solar energy conversion due to their strong light scattering effects and high surface-to-volume ratio. The highly ordered, vertically oriented tubular structure is very suitable for a high degree of electron mobility along the tube axis, perpendicular to the substrate, which will greatly reduce interface recombination. Fig. 1 shows the electron transporting pathways in a nanocrystalline TiO_2 film and the ordered TiO_2 NT arrays. The anodized tube structures are expected to greatly improve the charge collection efficiency due to directional electron conduction with minor charge recombination in comparison to TiO_2 nanoparticle films.[28] Moreover, the enhanced internal and external surface area is available for more dye loading,[50] particularly in TiO_2 nanotube-based photoelectrodes, where two solar cell architectures are paid significant research interest: sensitized solar cells and TiO_2/polymer solar cells.[51,52]

2. Anodized TiO_2 nanotubes

2.1 Conventional TiO_2 nanotubes

In 1999, Zwilling and co-workers first reported the TiO_2 porous film by anodic oxidation of a titanium sheet at low voltage.[53,54] Benchmark anodized TiO_2 nanotube arrays were initiated by the Grimes group in 2001, in which the nanotubes were formed in an HF aqueous electrolyte with lengths up to 0.5 μm.[55] Compared with the hydrothermal or template approach,[56–59] anodic oxidation is a more simple and convenient method to obtain uniform and orderly arranged nanotubes perpendicular to the substrate with controllable pore size and length.

Basically two simultaneously occurring reactions are involved in the anodization process: 1) the electrochemical dissolution of Ti under a potential induces complexation with fluoride ions, anodization speed ($\upsilon_{electro}$); 2) Chemical reaction based dissolution of the ejected $Ti(OH)_4$ at the entrance of the NTs, chemical etching speed (υ_{dis}). When $\upsilon_{electro}$ is much larger than υ_{dis}, the porous TiO_2 nanotube arrays will form and the tube length will gradually increase with time. When $\upsilon_{electro}$ is slightly larger than υ_{dis}, self-supporting TiO_2 nanotubes appear; when υ_{dis} is much faster than $\upsilon_{electro}$, free-standing NTs develop. The fabrication process of these two kinds of TiO_2 NTs and possible anodization mechanism are shown in Scheme 1, where localized chemical dissolution and field-assisted oxidation are shown to precisely determine the final nanoscale architecture.[60]

When the growth and dissolution rate reach a balance, the length of TiO_2 NTs will not increase, even if the oxidation time is increased. The barrier layer migrates to the metal substrate to achieve the growth of nanotubes, while chemical dissolution leaves the nanotubes shorter and between these two processes, the growth speed of TiO_2 nanotubes is determined.[25,61] A faster migration speed of the barrier layer and a slower chemical dissolution rate results in longer tubes, while a greater dissolution effect can decrease the tube length.[62] Thus, by precisely regulating the anodization conditions we can effectively control the nanotube morphology to preferred diameters and lengths.

The initial fabrication of TiO_2 NTs was in an aqueous solution containing hydrofluoric acid, because the chemical dissolution rate was too high, the NTs were very short.[55] A neutral fluoride solution containing phosphate was reported by Schmuki *et al.* for the preparation of TiO_2 NTs, in which the low acidity environment led to a tube length of up to 4 μm.[63] Afterwards, Schmuki and Grimes groups used organic solutions as the electrolyte to prepare TiO_2 NTs with even longer thickness and unprecedented regularity.[64,65] The tube lengths were extended to 134 and 360 μm,[66,67] by the choice of proper anodization conditions, the length can even reach 1000 μm and the aspect ratio up to 10 000.[68] Conventional TiO_2 NTs were often prepared at constant-voltage conditions at a slow growing rate due to the decreased current density during the anodizing process and the appearance of a thick insulating oxide layer. To prepare high aspect ratio TiO_2 NTs in a short time, a hybrid two step anodic strategy was introduced: first, constant-voltage anodization which is then followed by constant-current anodization.[69] Besides fluoride ions,[70,71] chlorine or bromide-based electrolytes are also suitable for TiO_2 NT growth.[72–75] So far, the most commonly used organic electrolyte is ethylene glycol,[76] glycol,[77] water-free acetic acid[78] and dimethyl sulfoxide (DMSO).[79,80] Most of the TiO_2 nanotubes are obtained in solutions containing fluorinated electrolytes. The fluoride ions are essential because they can react with TiO_2 to form water-soluble $[TiF_6]^{2-}$ complexes to remove the unwanted precipitate, which is the major driving force for developing tubular structures.

2.2 Top porous TiO_2 nanotubes

Generally, the chemical dissolution reaction helps to remove the ejected $Ti(OH)_4$, which results in clear, free standing nanotubular morphology. When the dissolution reaction is weak, the sealing of nanotube by the ejected $Ti(OH)_4$ is common. In most studies, the morphology of TiO_2 NTs is not regular enough and many defects are present, such as bundling, sealing, over-etching or cracks, which seriously affect its photoelectric properties. This is largely because it is difficult to find a proper balance between the two simultaneously occurring reaction steps. With increasing aspect ratios of TiO_2 NTs, bundling becomes more obvious which will bring a greater chance of recombination in TiO_2 NT-based solar cells.[28,81,82] In TiO_2/polymer solar cells, surface bundling also leads to a large number of cracks on the top the surface, which is undesirable for building ordered p–n heterojunction structures. The sealing issue will seriously prevent the

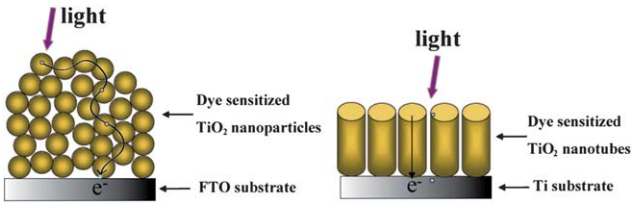

Fig. 1 A comparison of the electron pathways through nanoparticle and nanotubular structured TiO_2.

p-type materials from filling the nanotube interior. Over etching the pits can also lead to the aggregation of dyes and inadequate contact with the counter electrode in dye-sensitized solar cells, which can reduce the overall efficiency of the solar cells. Device optimization involves optimizing the anodizing conditions for the growth of regular, uniform nanotubes. Fig. 2 (a) shows one example of the bundling problem. When TiO_2 NTs grow very long, the tops will aggregate together, leaving large cracks that can be several hundreds of nanometres in width (see the reversed contrast of these cracks). Upon filling with the counterpart materials, when making a solar cell device, this will result in a large amount of the counterpart materials not working properly. The perfect configuration would be the interdigitated heterojunctions with a uniform distribution of materials.

The bundling is primarily caused by capillary force. Frank *et al.* have prepared nonbundling and crack-free NT films using supercritical CO_2 as the drying technique.[82] Inspired by the anodization of aluminium, in which nanoporous structures are mostly obtained, we have thought about making TiO_2 materials with a similar structure. Guided by the above mentioned anodization mechanisms, a too slow chemical etching rate results in surface precipitation, if the deposition of titanium oxide at the entrance of nanotubes is at a moderate rate: it accumulates but does not block the nanotube end and interconnected nanopores are formed,[83] and field-induced random dissolution of the surface forms pore-like structures which develop into tube-like structures.[84]

For this purpose, a novel two-step anodization was proposed to prepare perfectly aligned nanotubes, in which the first step is the traditional anodization of prepared TiO_2 nanotube arrays in ethylene glycol containing a small amount of ammonium fluoride (NH_4F), then the TiO_2 nanotube array films can be easily removed by simple sonication in acidic aqueous solution, leaving bowl-like footprints on the titanium substrate. After the second anodization, still in the same electrolyte but with the addition of a small amount of hydrofluoric acid (HF), perfectly aligned top porous TiO_2 NTs can be formed, free of over-etching, bundling and pore sealing, leaving the structures suitable for a secondary material deposition, Fig. 2(b, c) are the surface and cross-section images of porous TiO_2 NTs by a two-step anodization, respectively. The two-step anodization process shows good potential for the large-scale production of TiO_2 nanotube array films that could be used as photoelectrode materials and therefore, the large-scale production of TiO_2 nanotube based solar cells is possible. According to some detailed general studies, a low temperature, high voltage, a relatively short oxidation time and a low acid concentration are suitable for preparing porous TiO_2 NTs in ethylene glycol.[60] Additionally, electrolyte composition also plays a critical and important role in determining the resultant morphology of nanotubes, for example, in aqueous solutions, the anodization potential plays a significant role in the nanotube formation, but in nonaqueous solutions, the temperature becomes the major factor to govern the nanotube growth.[85]

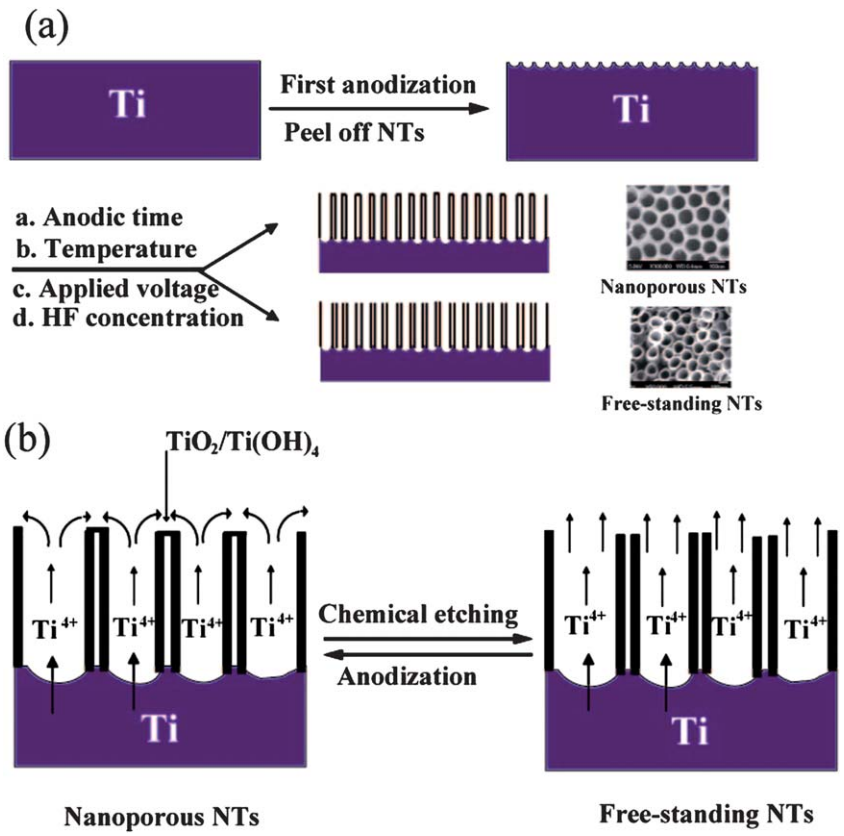

Scheme 1 (a) The controllable fabrication process of TiO_2 nanotubes by adjusting the reaction conditions; (b) The possible formation mechanism of nanoporous and free-standing TiO_2 nanotubes.

2.3 Fabrication of TiO_2 NTs on transparent substrate

The backside-illumination mode of anodized TiO_2 nanotube-based solar cells is an

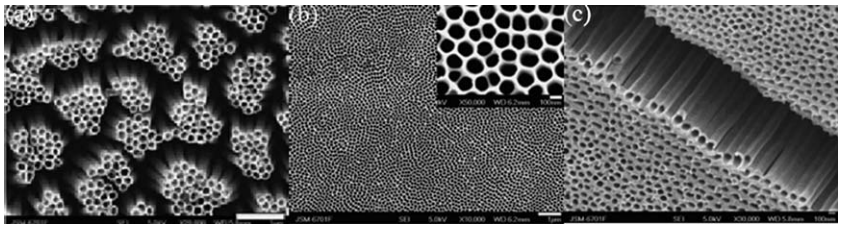

Fig. 2 (a) FE-SEM morphology of TiO_2 NTs by conventional anodization; (b) Top view of porous TiO_2 NTs; (c) Cross-section view of TiO_2 NTs, porous morphology on the surface and nanotubes underneath.

obstacle for realizing a high-efficiency since the redox electrolyte containing the iodine species has an absorption in the near UV spectrum and the platinum coated FTO partially, and inevitably reflects light. The relatively low photovoltaic performance of TiO_2 NT-based solar cells partly comes from an inability to fabricate high quality TiO_2 NTs on a transparent conductive substrate. Thus, fabricating TiO_2 NT arrays on a transparent substrate for front-side illumination is required to avoid a loss of light and attain higher power-conversion efficiencies (Fig. 3(a)).[86]

Preparing TiO_2 NTs on transparent conductive oxides (TCO) has gained a lot of interest recently, mainly involving either the transfer of the TiO_2 NT films on conductive glass[87–89] or direct titanium anodization on transparent conductive substrates.[86] Fig. 3(b) represents a typical process of fabricating TiO_2 NT films on FTO, which involves detaching the TiO_2 NT membrane from the Ti foil *via* ultrasonic treatment, then transferring and adhering the membrane onto FTO glass.[90] Several strategies have been developed to separate TiO_2 nanotube films from Ti substrates in order to obtain freestanding TiO_2 nanotube arrays, such as soaking in HCl solution with ultrasonic treatment or in a saturated $HgCl_2$ solution,[60,83] using a H_2O_2 solution to resolve the underlayer TiO_2 for separation,[88] through the evaporation of methanol to delaminate the barrier layer of the TiO_2 followed by a small amount of bending of the anodized Ti foil to detach it.[91] However, because of the fragile nature of the anodized TiO_2 membrane, it is difficult to ensure the integrity during the transfer process and large scale production can be a problem. Electrochemical growth of TiO_2 nanotubes on a transparent conductive substrate (FTO) coated with a Ti layer will solve this problem. Grimes and co-workers sputtered a 500 nm thick titanium film on fluorine-doped tin oxide (FTO) through radio-frequency magnetron sputtering,[86] with the increase in the thickness of titanium film, a very long vertically aligned TiO_2 NT layer can be achieved on FTO.[92] For direct growth of the TiO_2 nanotube film, electroetching of the Ti layer should be complete, otherwise the leftover Ti film will impede any light passing through. How to further increase the sputtered Ti films on FTO and optimize the anodization conditions for perfectly arranged TiO_2 NTs with the desired lengths and diameters is still worth investigating.

3. Applications in solar cells

3.1 Strategies of sensitization

The band gap of anatase TiO_2 is approximately 3.2 eV, corresponding to 387.5 nm in the ultraviolet region and overlaps with many solar absorbing dyes, making it a very good photoanode material. The TiO_2 and dye combination is one of the most important in utilizing solar energy and can extend the absorption spectrum to the visible region. The sensitizers that are effective with TiO_2 include organic dyes,[93,94] narrow band gap nanocrystalline such as CdS,[95] CdSe,[96] and sensitization through atom doping to the lattice of crystalline TiO_2 is also viable.[97]

Organic dye-sensitized solar cells. The conceptual dye-sensitized solar cell (DSSC) was first reported by Grätzel *et al.* in 1991, who used organic dye-sensitized nanocrystalline TiO_2 porous films as the photoanode and redox pair reactions of I_3^-/I_2 couples to complete the circuit and an initial efficiency of 7.1%–7.9% was obtained.[98] Since then, considerable efforts have been devoted to designing new dyes with increased molar absorption coefficients for visible light harvesting over the entire spectrum, and impressive solar cells efficiencies of 6%–11% have been gained.[99–105] Fig. 4 shows the structures of some typical organic dyes, the most efficient DSSCs so far still uses Ru-based dyes such as N3 and N719, with which the efficiency has been boosted over 11%.[106,107] C101, as shown in Fig. 4, has a very high molar extinction coefficient in acetonitrile-based electrolytes, and is used to achieve a strikingly high efficiency of 11.0–11.3%. Using low volatility 3-methoxypropionitrile electrolyte or solvent-free ionic liquid electrolytes to fabricate solar cells, the efficiencies can be stably retained at about 9.0% and 7.4% respectively even after 1000 h full sunlight soaking at 60 °C.[108] Another new dye, C104, with a higher molar extinction coefficient and excellent photochemical and thermal stability has been verified.[109] These trials will greatly advance the practical applications of DSSCs.

Developing new dyes with high molar absorption coefficients and a wider coverage of the solar spectral range is an ideal design for high-efficiency DSSCs,[110,111] which can be realized by synthetic chemistry to tune the absorption range to the visible region and even to the infrared range. On the other hand, the surface modification of TiO_2 materials is also promising in improving the efficiency of solar cells, such as COOH-functionalized Si nanoparticles[112] and graphene incorporation,[113] by which the charge transfer can be greatly facilitated.

As stated above, using anodized TiO_2 nanotubes in DSSCs will shorten the electron transport distance and reduce recombination. Schmuki and co-workers demonstrated the first anodized TiO_2 nanotube-based DSSCs, which uses N3 dye as the sensitizer, opening a new page for TiO_2 NT-based DSSCs.[114] The overall efficiencies have reached 2%–3% by using different lengths of TiO_2 NTs with a more defined geometry,[115] which is still far behind the conventional TiO_2 nanocrystalline film-based DSSCs. In order to expand the applications of TiO_2 NTs in DSSCs, perfectly ordered microstructures are required. Firstly, newly developed dyes should be tried with optimized conditions such as dye sensitization duration, concentration and annealing

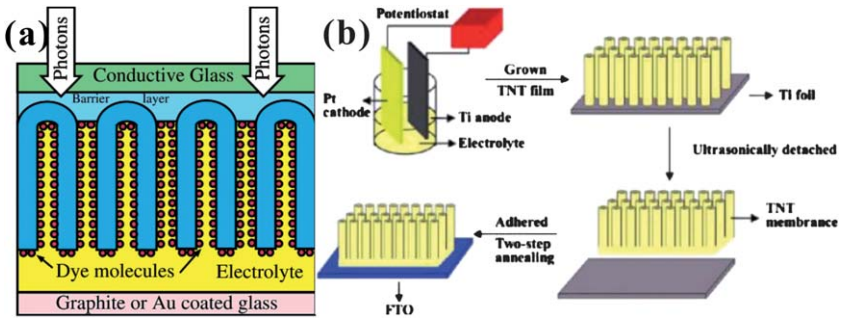

Fig. 3 (a) Frontside illumination, integration of transparent nanotube array architecture into dye solar cell structure; (b) Schematic illustration of the procedure for fabricating crystallized TNT/FTO glass films.

temperature *etc.* Ideally, dyes should cover TiO_2 in as an large area as possible to ensure a closely packed monolayer without aggregation.

In TiO_2 nanotube-based solar cells, the tube length and pore size has a direct influence on the solar cell performance. According to previous studies, by varying the tube length from 1 μm to 20 μm, the IPCE value increases gradually and attains a maximum value of 80% when the tube length reaches 20 μm.[116] Other research shows that the overall efficiency of DSSCs reaches 2.88% using 20 μm tubes and is higher than the 10 μm and 30 μm tubes, which show efficiencies of 2.33% and 2.87% respectively. It is speculated that 20 μm is the optimum tube length for the highest efficiency as more electrons are photogenerated and there is reasonable electron transport distance. Too short a length cannot provide a large enough surface area to adsorb enough dye in the solar cell devices. Further increasing the tube length could result in the higher resistance between the TiO_2 nanotubes layer and the Ti substrate, inducing more recombination sites that have a detrimental effect on the charge transport for longer tubes. Pore size is yet another significant parameter affecting the photo conversion efficiency. Previous studies have shown that for the same thickness of nanotube, reducing the pore size helps to improve the efficiency, which can be attributed to the enhanced specific surface area under a certain area of TiO_2 nanotubes.[26,115–117]

Quantum dot (QD) sensitized solar cells. Although sequential organic dyes in TiO_2 photoelectrodes are ideal to extend the range of light absorption in DSSCs,[118,119] attempts to lower the cost and improve the stability of DSSCs for practical applications, still meet with limited success. Some low band gap semiconductor nanocrystals such as CdS[120] or CdSe quantum dots[121] can significantly improve the solar cell stability, and the material properties can be tailored by quantum confinement to alter the band gap for a wider spectrum response. These QDs adsorbed onto TiO_2 materials have the capability of harvesting visible light so as to excite the electrons to their conduction band. The key requirement to transport the excited electrons to TiO_2 is that the energy level of the conduction band is slightly higher than the conduction band of TiO_2, which is the main driving force for the efficient charge injection. Fig. 5(a) shows the energy levels of some semiconductors, which provides the basis for choosing the possible semiconductors to sensitize TiO_2 materials. For example, CdS has the band gap of 2.25 eV, and the energy level of the conduction band is higher than TiO_2, so it can be an effective sensitizer for narrowing the band gap of TiO_2.[122] Fig. 5(b) shows how the charge transfer process between CdS and TiO_2 occurs: CdS absorbs sunlight and the electrons of CdS are excited to the conduction band, then the excited electrons are injected into the conduction band of TiO_2 for transporting the electrons to the external circuit. The process mainly relies on the slightly higher energy level of CdS compared to TiO_2, which can accelerate the charge transfer between CdS and TiO_2. The advantage of using QD sensitizers is that their band gaps can be tuned by changing the size of nanoparticles, providing new opportunities to extend the absorption spectra into a wider region.[123,124] PbS,[125] Bi_2S_3,[126] InAs,[127] In_2S_3[128] and $CuInS_2$[129] have been extensively used in quantum dot sensitized solar cells. With proper surface modification, both charge injection and recombination dynamics can be tailored to increase the efficiency.[130]

Semiconductor nanocrystals can be deposited inside TiO_2 nanotubes *via* chemical bath deposition. For example, alternated immersion in solutions of $CdSO_4$ and Na_2S can generate CdS nanocrystals on the walls of TiO_2 nanotubes.[131,132] Moreover, cathodic reduction,[133] close space sublimation technique,[134] organic linker assisted

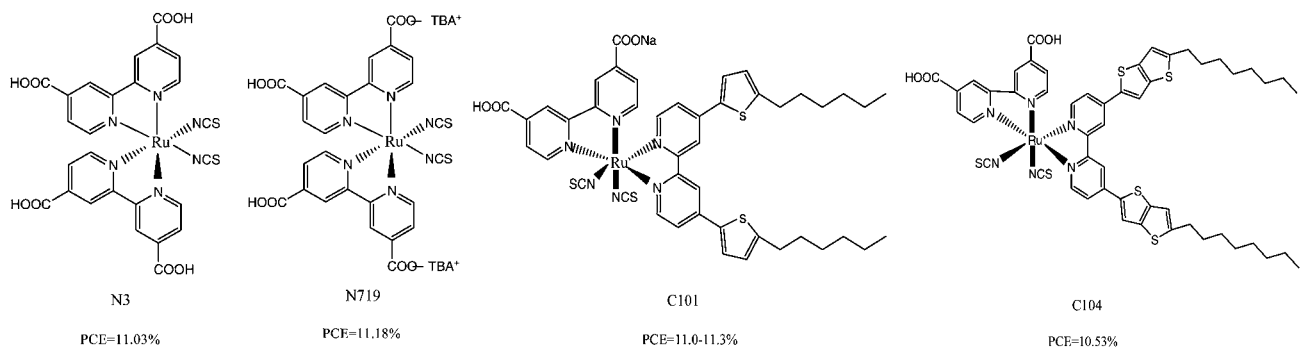

Fig. 4 Some efficient organic dyes and the corresponding photo conversion efficiencies.

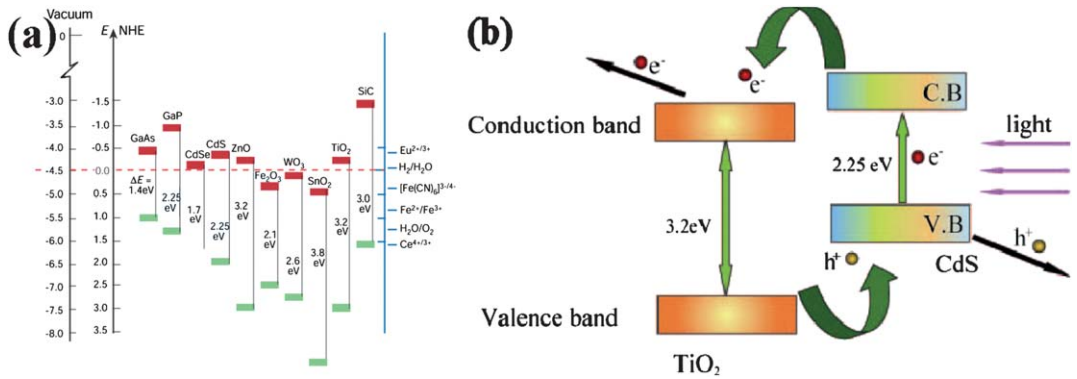

Fig. 5 (a) Band positions of several semiconductors in contact with an aqueous electrolyte at pH 1; (b) Schematic of the charge transfer process between CdS and TiO_2.

deposition,[135,136] spray pyrolysis deposition[137] and electrochemical atomic layer deposition[138] are also proposed in sensitizing TiO_2 nanotubes. Scheme 2 represents a typical sensitizing process by using an organic anchor to enhance the absorption of nanocrystals onto the TiO_2 NT walls.[136] The CdS sensitized TiO_2 nanotubes have attained a promising overall efficiency of 4.15% from photoelectrochemical cells.[131]

In QD solar cells, photodegradation of QDs should be seriously considered for prolonging the usage lifetime. Through coating a thin film of amorphous TiO_2 around the CdS QDs sensitized electrode, both the solar cell performance and photostability are greatly improved: the solar cell efficiency reaches 1.24% with an amorphous TiO_2 coating, but only 0.13% without the TiO_2 coating, which indicates that the amorphous coating can be used to effectively block charge recombination paths. The short circuit current density of non-coated photoelectrodes gradually decreases with time using periodic illumination intervals, but the coated one shows no decay, ascribed to the passivation effect on the QD surface states.[139,140] In addition, ZnS has also been used as a passivation coating to prevent QD nanocrystals from photocorrosion.[141,142] The energy gap of CdSe is another candidate for solar cells applications, but its band gap of 1.7 eV dictates the light response falling only in visible region. Exploring low band gap semiconductors such as PbS (0.41eV) can extend the solar spectrum to the near-infrared region,[135] and can thus be used for sensitizing TiO_2 NTs.

Co-sensitization. Absorption spectrum matching is an essential prerequisite for the realization of highly efficient solar cells. A single sensitiser may not be able to achieve the entire absorption of solar spectrum, co-sensitization using two or more sensitizers has been proposed as an important design feature, which allows for a greater degree of solar light absorption,[143–145] due to their different band gaps. For example, the band gap of CdS in bulk is 2.25 eV, meaning that only solar light below a 550 nm wavelength can be absorbed, while CdSe nanocrystals can extend the spectral absorption to 720 nm due to their relatively low band gap of 1.7 eV. However, the electron injection efficiency of CdSe is lower than CdS because its conduction band edge is below TiO_2, which is detrimental to the electron transfer between CdSe and TiO_2. To combine their respective advantages for strong light harvesting with a high electron injection efficiency, CdS and CdSe are used to co-sensitize a TiO_2 photoelectrode and the efficiency can be dramatically enhanced. When CdS and CdSe were used to sensitize TiO_2 in solar cells with a cascade structure, the Fermi level alignment occurred for redistributing these energy levels, both the energy levels of conduction and the valence bands of these three materials shows the order of TiO_2 < CdS < CdSe. Therefore, under the solar light illumination, the TiO_2/CdS/CdSe configuration exhibits a higher driving force for the injection of excited electrons, ascribing to the insertion of a CdS layer between TiO_2 and CdSe, which elevates the conduction band edge of CdSe, as shown in Fig. 6(a). The excited electrons transfer from CdSe to CdS, then inject into the conduction band of TiO_2, and the hole transfer complies with the reversed pathway. Fig. 6(b) represents the increased IPCE after CdS and CdSe quantum dot co-sensitization.[141] It also shows that a different cascade combination of TiO_2/CdSe/CdS has a very poor performance.

Doping. External sensitizers easily detach from the TiO_2 surface, especially in highly corrosive and oxidizing environments. Doping has proved critical for optimizing charge separation and transport in the TiO_2 bulk phase for narrowing the band gap to achieve visible absorption.[146,147] Several metal or nonmetal elements are used as the doping agent to reduce the bandgap of TiO_2, which can be realized by introducing impurities into the TiO_2 crystal lattice so as to change the band gap of TiO_2 or create new energy levels for visible light absorption.[148] Various elements, C,[147] N,[146] I,[149] and Nb[150] have been incorporated into the TiO_2 bulk phase to improve the photoelectric properties, and the doped-TiO_2 exhibits enhanced stability. Till now, doped-TiO_2 nanomaterials have not been widely studied in photoelectrical catalysis, and their abilities as potential solar cell materials will justify more trials.

3.2 TiO_2 nanotubes based polymer solar cells

Polymer solar cells based on fullerene derivatives and conducting polymers have received widespread attention in recent years because of the their easy industrial production by solution-based roll-to-roll process.[151–153] Fullerene derivatives with a high electron affinity can be used as a strong electron accepter material which, coupled with p-type conducting polymers (for example, poly-3-hexylthiophene,

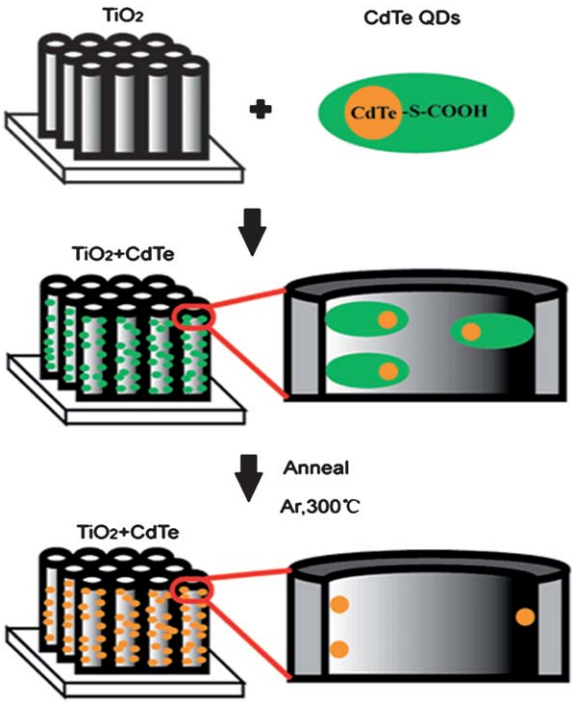

Scheme 2 The process of linking CdTe QDs to TiO_2 nanotubes.

P3HT) to make heterojunction solar cells[154–159] achieved efficiencies of 4.5%–6%.[160–162] By making a tandem solar cell architecture, the efficiency can be improved to over 6%.[163–165] TiO_2, as a significantly cheaper electron accepter material, can replace the fullerene derivatives to create hybrid solar cells. Another driving force is that to form ordered heterojunction solar cells using conducting polymers and fullerene derivatives to further enhance the efficiency still remains a great challenge. TiO_2 nanotubes provide a great opportunity to make ordered heterojunction solar cells in combination with p-type conducting polymers.

The traditional way to make the device is to blend nanostructured TiO_2 and the conducting polymer (P3HT) to building up random hybrid p–n structures.[52] Interface compatibility would be a key issue for hybrid p–n junctions that are prone to phase separation as it will inhibit the exciton separation, which would be more serious under long term storage under thermal or electrical stress. To improve the interfacial bonding strength, a self-assembly strategy was introduced to anchor carboxylated polythiophene onto the surface of TiO_2 by carboxylic groups (Scheme 3(a)), the charge separation efficiency was greatly enhanced and it produced an overall efficiency of 2.1%.[166] Other studies focus on engineering the surface of TiO_2 nanorods, which use dyes as an interface layer between TiO_2 and P3HT,[167,168] and *in situ* polymerization inside the TiO_2 nanotubes to provide better interface contact and higher coverage.[169]

The physical adsorption between an inorganic phase (TiO_2) and an organic one (conducting polymer) is probably not strong enough for the long term operation of solar cells, considering the incompatibility of the two phases. Direct chemical bonding becomes necessary to increase the interfacial adhesion strength. Surface initiated polymerization on the surfaces of TiO_2 is a good solution to the issue, where the conducting polymer is grown directly from the TiO_2 surface, resulting in a perpendicular chain orientation and the chemical bonding of the conducting polymer to the TiO_2 surface.[170,171] For example, the chain-growth surface-initiated Kumada catalyst-transfer polycondensation was introduced to grow P3HT on silica surfaces for the fabrication of nanostructured hybrids between conjugated polymer and inorganic materials, as shown in Scheme 3(c), which shows a potential use in the development of heterojunction solar cells.[172] A biomimetic catecholic monolayer containing pyrrole units was anchored onto a TiO_2 nanotube, a very useful technique for initiating surface electrochemical polymerization inside nanoporous TiO_2 nanotubes to make coaxial p–n nanohybrids in one step (Scheme 3(b)). These chemically attached p–n heterojunctions significantly improve the interfacial contact between p-type conducting

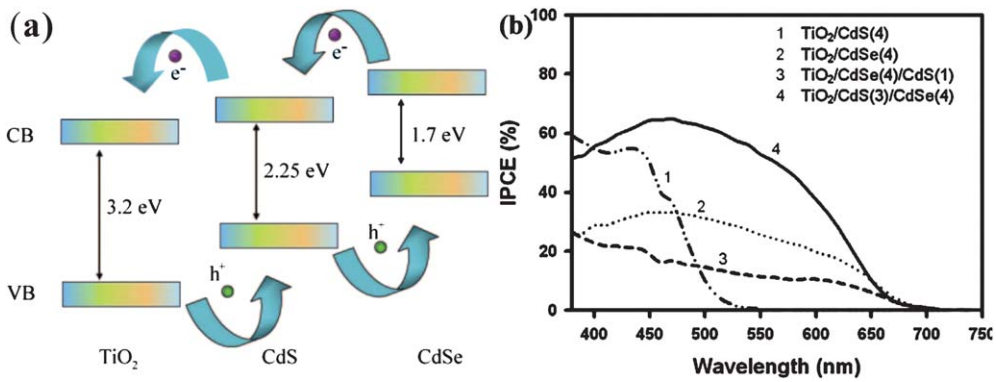

Fig. 6 (a) Ideal stepwise band edge structure for the efficient transport of the excited electrons and holes in a CdS/CdSe co-sensitized TiO_2 electrode; (b) IPCE curve: various QD-sensitized TiO_2 electrodes.

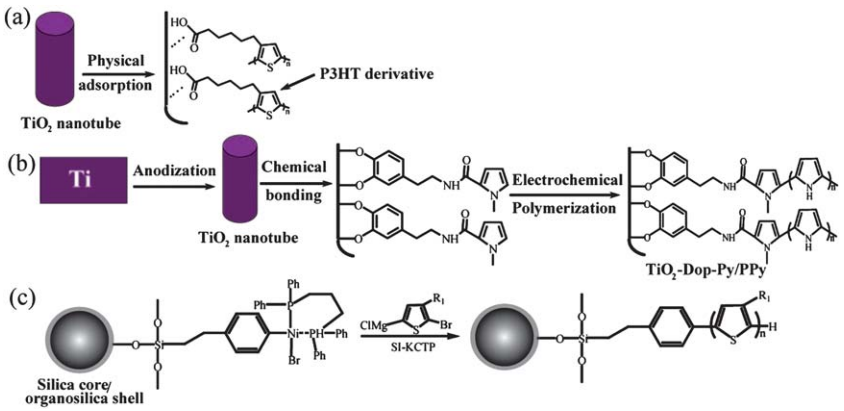

Scheme 3 (a) A schematic diagram of carboxylated P3HT self-assembled onto TiO_2 nanotube arrays; (b) Schematic representation of the electrochemical polymerization of PPy to construct chemically bonded p–n heterojunctions; (c) Surface-initiated Kumada catalyst-transfer polycondensation for preparing hairy P3HT particles.

polymers and TiO_2, which is easily concluded from an electrochemical impedance spectroscopy experiment: with the modification of the biomimetic anchor, the charge-transfer resistance decreased.[173] Chemical bonding will not only improve the interfacial contact and achieve a greater surface coverage of TiO_2, but also bring about direct bonding which will shorten the electron transporting distance with minimal loss. Preparing conductive polymers on some substrates holds potential applications in hybrid solar cells, but how to effectively initiate surface polymerization of the target monomer and control over the architectures still remains a challenging problem.

4. Strategies for optimizing the structure of TiO_2 NTs

Until now, the highest efficiency for pure TiO_2 nanotube-based DSSCs is about 4%,[26] which is far less than that for nanocrystalline TiO_2 porous film, which has shown efficiencies of over 11%.[107] The relatively low surface area of the nanotubes is responsible for the relatively low efficiency, in addition, the crystallinity should be improved and defects avoided during anodization.

4.1 Approaches for enhancing surface area

Secondary structures *via* $TiCl_4$ treatment. Anodized TiO_2 NTs always have relatively smooth tube walls, so one aspect of research would be to improve the surface area so that more charge separation interfaces can be created to increase the sunlight absorption, which results in a higher charge-separation efficiency. For that, TiO_2 nanoparticles can be attached onto both the outer and inner tube walls to create secondary structures, which is realized by either $TiCl_4$ treatment[174] or direct immersion in an aqueous solution of TiO_2 nanoparticles.[175] After treatment, more dye loading can be expected. Fig. 7(a–d) shows that after $TiCl_4$ treatment, TiO_2 nanoparticles are uniformly distributed on both surfaces which enables the tube walls to absorb a greater amount of dye. Obviously, $TiCl_4$ treatment yields a significantly enhanced photocurrent density and results in a 5 times greater efficiency over non-treated nanotubes.[86](Fig. 7(e)) In addition to oxygen plasma treatments, dye-sensitized TiO_2 nanotubes exhibited an overall efficiency (PCE) of 7.37% under backside illumination.[176] The creation of secondary structures can be further optimized, for example, anodizing micro-patterned titanium.

Micro-patterned TiO_2 nanotubes. To further increase the specific surface area, a new strategy of engineering the titanium surface *via* laser micro-machining techniques, combined with conventional anodization is designed to fabricate TiO_2 NTs arrays on a microstructured titanium substrate. Fig. 8 shows the SEM and FESEM images of the patterned titanium before and after anodization, the TiO_2 NTs distribute on both the bottom surfaces and sides.[177] These patterned TiO_2 NTs can greatly enlarge the surface areas and result in an enhanced IPCE and photocatalytic ability. Moreover, the microstructures greatly improve the mechanical property of TiO_2 NT films on mother Ti substrates, probably due to the scattered internal stress inside NT films.

Novel morphology by adjusting anodization conditions. A TiO_2 mesosponge was prepared *via* a new anodization approach and selective etching strategy which can be used for high-efficiency DSSCs and photocatalysis,[178,179] Fig. 9(a, b) shows the TiO_2 mesosponge layers *via* unconventional anodization. Two different constant voltages, with cycle scanning, was used for the anodization which was performed to fabricate bamboo-type TiO_2 nanotubes, this novel structure provides a large amount of space for dye loading in solar cells.[180] (Fig. 9(c, d)) Different from conventional anodization, the first anodization is carried out in a salt solution (NaCl) to construct microstructured titanium surfaces for enhanced surface roughness, and the second process is conventional anodization for the growth of the nanotubes.[181] These hierarchical micro- and nanostructures on the Ti surface (Fig. 9(e, f)) have the potential to increase the surface area for more dye loading in solar cells. TiO_2 nanotubes can be easily anodized, and TiO_2 nanowires and nanoplates are also easily prepared, which provides a simple methodology for fabricating various TiO_2 nanostructures.[182] Further optimization of the nanotubes by changing the anodization parameters still has the opportunity to improve the performance of this material when used for solar cell devices.

4.2 Improving crystallinity

The crystalline form of TiO_2 is crucial in determining the performance of solar cells. Anodized TiO_2 nanotubes often possess negligible photoelectric properties due to their amorphous, crystalline structure. The crystalline form of TiO_2 mainly depends on the annealing temperature which can have a significant influence on the photoelectric response.[183] Annealing at a proper temperature can not only improve the crystallinity, but will also reduce the gap of the grain boundaries and facilitate the connectivity

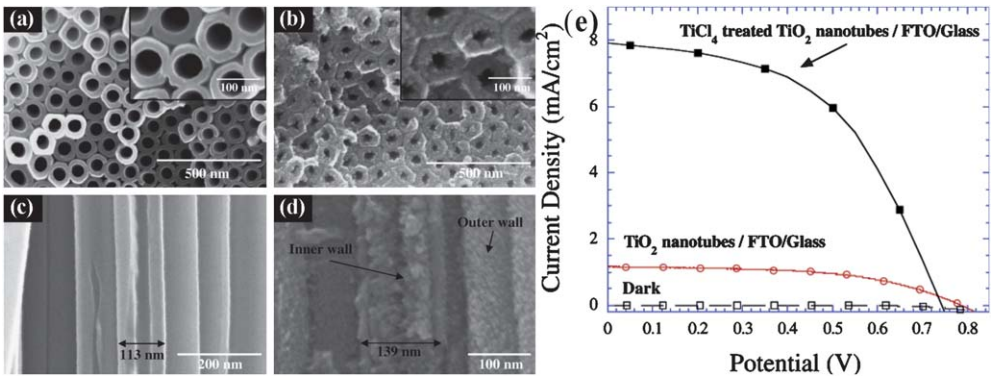

Fig. 7 SEM images of TiO_2 nanotubes before (a, c) and after $TiCl_4$ treatment (b, d); (e) Photocurrent–photovoltage characteristics of a transparent nanotube array DSC under 100% AM-1.5 illumination.

between grains and eliminate the charge recombination sites. The temperature of 450–500 °C is the best range for anatase formation, while above 550 °C, a rutile phase appears which is not beneficial for electron conduction.[117] So controlling the sintering conditions to keep the TiO_2 materials as pure anatase crystals is crucial for the fabrication of high performance photovoltaic devices.

5. Flexible TiO_2 nanotube solar cells

Transparent conductive glass is the most commonly used substrate to deposit TiO_2 nanocrystalline film onto as the photoelectrode, but the poor toughness does not allow the production of flexible devices. Flexible substrates such as plastic materials or flexible metals can be used to replace FTO for flexible device applications.[184]

Nanocrystalline TiO_2 particles on a flexible substrate

Plastic materials can be used for flexible DSSCs, but poor stability limits their applications in chemically corrosive and high-temperature environments. Metal sheets, like stainless steel[185] or titanium[186,187] can be also used to fabricate flexible DSSCs.

Top porous TiO_2 nanotube based flexible coaxial nanohybrids

Because of the internal stress, TiO_2 nanotube films can usually be easily peeled-off from the Ti substrate. They are very fragile either on a titanium substrate or as a self-supporting film. One approach to enhance the toughness of the material is to incorporate a soft phase to form interpenetrating structures to disperse the internal stress. Frank's group have reported the use of electrodeposition to fill the ordinary TiO_2 nanotubes with p-type materials.[188] However, conventional TiO_2 NTs are not a good template and the electrochemical reaction also occurred in the cracks and spaces among the tubes, which retards the formation of highly ordered p–n heterojunctions. Porous TiO_2 nanotubes with interconnected nanopores at the top and tubular structures underneath[83,189,190] only allow electrodeposition to occur inside the nanotubes, and form highly ordered p–n heterojunctions. These nanopores on the surface play the key role to restrict the electrodeposition to only the inside of the tubes, where metals (Ni), semiconductors (CdS) and conductive polymers (PPy) can be deposited to form nanohybrid materials. Fig. 10(a) is an SEM image of the top porous TiO_2 NTs, the hybrid materials are shown in Fig. 10 (b–e), and the optical image of coaxial TiO_2 NT-PPy nanowire materials in Fig. 10(f). Interestingly, the TiO_2/metal and TiO_2/PPy nanohybrids can be easily peeled off from Ti substrate and exhibit high flexibility. The composite film can be bent for many cycles without being cracked, which is amazing when compared with conventional fragile TiO_2 NTs. It is expected that the composite hybrid structures hold significant potential in the formation of highly ordered p–n heterojunction materials for flexible solar cell applications.[191]

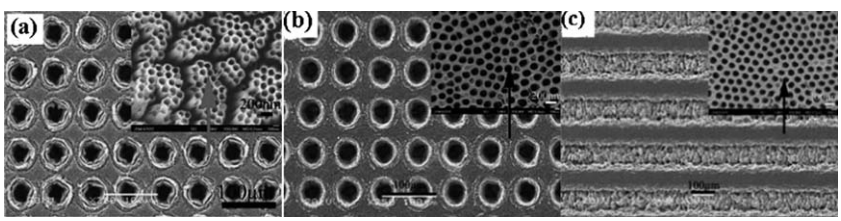

Fig. 8 The SEM and FESEM images of a patterned titanium substrate and TiO_2 nanotubes. (a) Free-standing TiO_2 nanotubes: patterned titanium after anodization at 60 V for 2 h, the insets are the FESEM images of the TiO_2 NT arrays; (b, c) Top porous TiO_2 nanotubes *via* a two step anodization, dot pattern and line pattern, respectively.

6. Summary and outlook

TiO_2 nanotube arrays on substrates (either Ti or transparent conducting glass) provide a superior platform for building up ordered heterojunctions for enhanced charge separation and electron transportation. The parameters of the TiO_2 nanotubes can be finely tuned, allowing the optimization of device fabrication for different types of solar cells, such as DSSCs and TiO_2 nanotube/polymer solar cells. Anodization conditions are being further optimized for desired structures, for example, tunable nanotube morphology, diameter, thickness and inter-tubular spacing, towards perfect alignment by the formation of top porous

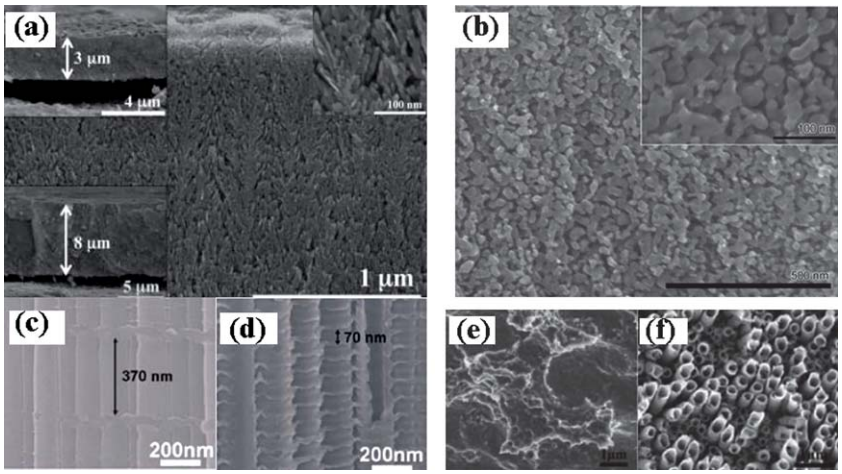

Fig. 9 (a) SEM image of the TiO_2 mesosponge layers formed on Ti by anodization. The upper and lower insets show TiO_2 mesosponge layers formed by anodization over 24 and 48 h, respectively. The inset on the top right is the magnified SEM image of the layer morphology; (b) SEM images after etching in 30 wt% H_2O_2 for 1 h, lead to a highly regular sponge morphology; (c, d) SEM image of bamboo-type tubes under different alternating voltage cycling conditions; (e) SEM image of microstructured Ti surface after the first anodization to improve the surface roughness; (f) SEM images of anodized TiO_2 nanotubes on microstructured Ti substrate.

nanotubes. In terms of the surface area, TiO_2 nanotubes are still incomparable with TiO_2 nanoparticles. Different strategies have been developed to enhance the surface area, such as double-walled tubes or bamboo-type nanotubes, the creation of secondary structures on smooth tube walls (TiO_2 nanoparticle decoration) or the fabrication of nanotubes on micro patterned substrates *etc.* A number of synthetic strategies have been developed to introduce nanocrystals or nanocrystal combinations onto TiO_2 to extend the spectrum absorption of TiO_2; to create chemical bonding between p-type conducting polymers and the TiO_2 surface. As some of the approaches have begun to establish, the next step would be to use them for targeted device design with interesting materials. With the advance of novel sensitized dyes with high extinction constants and good stability, these dyes deserve trials on novel TiO_2 nanotubular structures, so that their promising solar cell efficiencies can be explored. The deposition of p-type materials inside nanoporous TiO_2 NTs can form perfectly ordered p–n heterojunctions, which induces amazing flexibility in the TiO_2 NTs/polymer hybrids and is capable of fabricating flexible device in a single step. How to control the regularity during electrodeposition to enhance the conduction mobility remains a challenge and will require extensive trials.

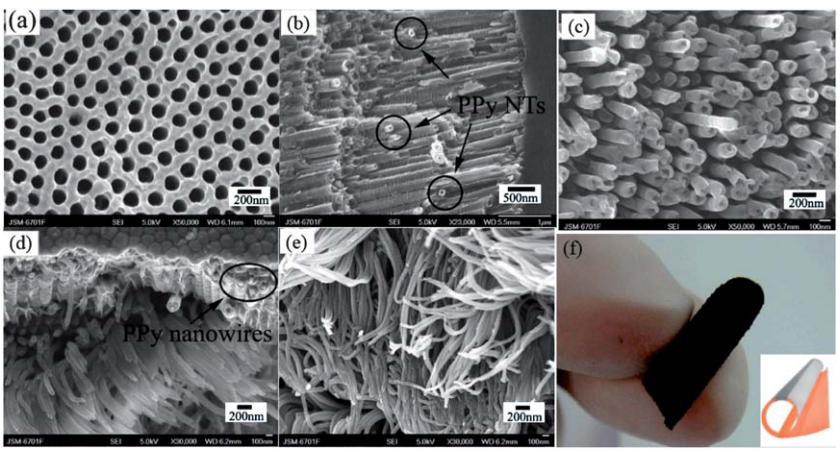

Fig. 10 FESEM images of top-porous TiO_2 NT arrays and PPy NTs and nanowires. (a) Top surface views of perfectly aligned porous TiO_2 NTs; (b, d) cross-sectional and bottom surface views of coaxial PPy-TiO_2 NTs and nanowires; (c) images of PPy NTs peeled off the substrates by mechanical force; (d) cross-sectional and bottom surface views of coaxial PPy-TiO_2 nanowires; (e) images of PPy nanowire self-supporting films after dissolving the TiO_2 NTs in an HF aqueous solution; (f) Optical images of the flexible, free-standing coaxial TiO_2 NT-PPy nanowire composite. The inset shows the schematic diagram of flexible coaxial nanohybrids.

Acknowledgements

Many thanks for the support of NSFC (20973188) and "Hundred Talents Program" of Chinese Academy of Sciences.

References

1 I. Gur, N. A. Fromer, M. L. Geier and A. P. Alivisatos, *Science*, 2005, **310**, 462–465.
2 P. Wang, S. M. Zakeeruddin, J. E. Moser, M. K. Nazeeruddin, T. Sekiguchi and M. Grätzel, *Nat. Mater.*, 2003, **2**, 402–407.
3 A. I. Hochbaum and P. Yang, *Chem. Rev.*, 2010, **110**, 527–546.
4 T. M. Clarke and J. R. Durrant, *Chem. Rev.*, 2010, **110**, 6736–6767.
5 W. Wu, J. Yang, J. Hua, J. Tang, L. Zhang, Y. Long and H. Tian, *J. Mater. Chem.*, 2010, **20**, 1772–1779.
6 Y. Luo, D. Li and Q. Meng, *Adv. Mater.*, 2009, **21**, 4647–4651.
7 W. Zeng, Y. Cao, Y. Bai, Y. Wang, Y. Shi, M. Zhang, F. Wang, C. Pan and P. Wang, *Chem. Mater.*, 2010, **22**, 1915–1925.
8 L. Huo, J. Hou, S. Zhang, H. Y. Chen and Y. Yang, *Angew. Chem., Int. Ed.*, 2010, **49**, 1500–1503.
9 D. Venkataraman, S. Yurt, B. H. Venkatraman and N. Gavvalapalli, *J. Phys. Chem. Lett.*, 2010, **1**, 947–958.
10 M. A. Franzman, C. W. Schlenker, M. E. Thompson and R. L. Brutchey, *J. Am. Chem. Soc.*, 2010, **132**, 4060–4061.
11 Y. Yu, P. V. Kamat and M. Kuno, *Adv. Funct. Mater.*, 2010, **20**, 1464–1472.
12 Y. Qiu, W. Chen and S. Yang, *Angew. Chem., Int. Ed.*, 2010, **49**, 3675–3679.
13 S. Wenger, P. A. Bouit, Q. Chen, J. Teuscher, D. D. Censo, R. Humphry-Baker, J. E. Moser, J. L. Delgado, N. Martín, S. M. Zakeeruddin and M. Grätzel, *J. Am. Chem. Soc.*, 2010, **132**, 5164–5169.
14 W. C. Sinke and M. M. Wienk, *Nature*, 1998, **395**, 544–545.
15 K. M. Coakley and M. D. McGehee, *Chem. Mater.*, 2004, **16**, 4533–4542.
16 F. Huang, D. Chen, X. Zhang, R. A. Caruso and Y. B. Cheng, *Adv. Funct. Mater.*, 2010, **20**, 1301–1305.

17 D. Fu, X. Zhang, R. L. Barber and U. Bach, *Adv. Mater.*, 2010, **22**, 4270–4274.
18 Z. Liu and M. Misra, *ACS Nano*, 2010, **4**, 2196–2200.
19 C. S. Rustomji, C. J. Frandsen, S. Jin and M. J. Tauber, *J. Phys. Chem. B*, 2010, **114**, 14537–14543.
20 U. Bach, D. Lupo, P. Comte, J. E. Moser, F. Weissörtel, J. Salbeck, H. Spreitzer and M. Grätzel, *Nature*, 1998, **395**, 583–585.
21 S. M. Feldt, E. A. Gibson, E. Gabrielsson, L. Sun, G. Boschloo and A. Hagfeldt, *J. Am. Chem. Soc.*, 2010, **132**, 16714–16724.
22 M. Grätzel, *Nature*, 2001, **414**, 338–344.
23 G. K. Mor, O. K. Varghese, M. Paulose, K. Shankar and C. A. Grimes, *Sol. Energy Mater. Sol. Cells*, 2006, **90**, 2011–2075.
24 K. Shankar, J. I. Basham, N. K. Allam, O. K. Varghese, G. K. Mor, X. Feng, M. Paulose, J. A. Seabold, K. S. Choi and C. A. Grimes, *J. Phys. Chem. C*, 2009, **113**, 6327–6359.
25 A. Ghicov and P. Schmuki, *Chem. Commun.*, 2009, 2791–2808.
26 P. Roy, D. Kim, K. Lee, E. Spiecker and P. Schmuki, *Nanoscale*, 2010, **2**, 45–59.
27 S. Rani, S. C. Roy, M. Paulose, O. K. Varghese, G. K. Mor, S. Kim, S. Yoriya, T. J. LaTempa and C. A. Grimes, *Phys. Chem. Chem. Phys.*, 2010, **12**, 2780–2800.
28 K. Zhu, N. R. Neale, A. Miedaner and A. J. Frank, *Nano Lett.*, 2007, **7**, 69–74.
29 T. S. Kang, A. P. Smith, B. E. Taylor and M. F. Durstock, *Nano Lett.*, 2009, **9**, 601–606.
30 F. Sauvage, F. D. Fonzo, A. L. Bassi, C. S. Casari, V. Russo, G. Divitini, C. Ducati, C. E. Bottani, P. Comte and M. Graetzel, *Nano Lett.*, 2010, **10**, 2562–2567.
31 Y. Qu, W. Zhou, K. Pan, C. Tian, Z. Ren, Y. Dong and H. Fu, *Phys. Chem. Chem. Phys.*, 2010, **12**, 9205–9212.
32 G. K. Mor, S. Kim, M. Paulose, O. K. Varghese, K. Shankar, J. Basham and C. A. Grimes, *Nano Lett.*, 2009, **9**, 4250–4257.
33 Q. Tai, X. Zhao and F. Yan, *J. Mater. Chem.*, 2010, **20**, 7366–7371.
34 Z. Jiang, F. Yang, N. Luo, B. T. T. Chu, D. Sun, H. Shi, T. Xiao and P. P. Edwards, *Chem. Commun.*, 2008, 6372–6374.
35 L. Yang, S. Luo, R. Liu, Q. Cai, Y. Xiao, S. Liu, F. Su and L. Wen, *J. Phys. Chem. C*, 2010, **114**, 4783–4789.
36 J. Zhao, S. Sallard, B. M. Smarsly, S. Gross, M. Bertino, C. Boissière, H. Chen and J. Shi, *J. Mater. Chem.*, 2010, **20**, 2831–2839.
37 T. W. Kim, H. W. Ha, M. J. Paek, S. H. Hyun, J. H. Choy and S. J. Hwang, *J. Mater. Chem.*, 2010, **20**, 3238–3245.
38 V. Etacheri, M. K. Seery, S. J. Hinder and S. C. Pillai, *Chem. Mater.*, 2010, **22**, 3843–3853.
39 G. Yang, Z. Jiang, H. Shi, T. Xiao and Z. Yan, *J. Mater. Chem.*, 2010, **20**, 5301–5309.
40 Z. Li, H. Zhang, W. Zheng, W. Wang, H. Huang, C. Wang, A. G. MacDiarmid and Y. Wei, *J. Am. Chem. Soc.*, 2008, **130**, 5036–5037.
41 N. K. Shrestha, J. M. Macak, F. Schmidt-Stein, R. Hahn, C. T. Mierke, B. Fabry and P. Schmuki, *Angew. Chem., Int. Ed.*, 2009, **48**, 969–972.
42 Y. Y. Song, F. Schmidt-Stein, S. Bauer and P. Schmuki, *J. Am. Chem. Soc.*, 2009, **131**, 4230–4232.
43 E. Balaur, J. M. Macak, H. Tsuchiya and P. Schmuki, *J. Mater. Chem.*, 2005, **15**, 4488–4491.
44 S. Caramori, V. Cristino, R. Argazzi, L. Meda and C. A. Bignozzi, *Inorg. Chem.*, 2010, **49**, 3320–3328.
45 K. S. Mun, S. D. Alvarez, W. Y. Choi and M. J. Sailor, *ACS Nano*, 2010, **4**, 2070–2076.
46 J. Zou, Q. Zhang, K. Huang and N. Marzari, *J. Phys. Chem. C*, 2010, **114**, 10725–10729.
47 M. Pagliaro, G. Palmisano, R. Ciriminna and V. Loddo, *Energy Environ. Sci.*, 2009, **2**, 838–844.
48 A. Kongkanand, K. Tvrdy, K. Takechi, M. Kuno and P. V. Kamat, *J. Am. Chem. Soc.*, 2008, **130**, 4007–4015.
49 D. R. Baker and P. V. Kamat, *Adv. Funct. Mater.*, 2009, **19**, 805–811.
50 K. Shankar, J. Bandara, M. Paulose, H. Wietasch, O. K. Varghese, G. K. Mor, T. J. LaTempa, M. Thelakkat and C. A. Grimes, *Nano Lett.*, 2008, **8**, 1654–1659.
51 D. Kuang, J. Brillet, P. Chen, M. Takata, S. Uchida, H. Miura, K. Sumioka, S. M. Zakeeruddin and M. Grätzel, *ACS Nano*, 2008, **2**, 1113–1116.
52 Z. J. Wang, S. C. Qu, X. B. Zeng, J. P. Liu, C. S. Zhang, F. R. Tan, L. Jin and Z. G. Wang, *Appl. Surf. Sci.*, 2008, **255**, 1916–1920.
53 V. Zwilling, E. Darque-Ceretti, A. Boutry-Forveille, D. David, M. Y. Perrin1 and M. Aucouturier, *Surf. Interface Anal.*, 1999, **27**, 629–637.
54 V. Zwilling, M. Aucouturier and E. Darque-Ceretti, *Electrochim. Acta*, 1999, **45**, 921–929.
55 D. Gong, C. A. Grimes and O. K. Varghese, *J. Mater. Res.*, 2001, **16**, 3331–3334.
56 Z. R. Tian, J. A. Voigt, J. Liu, B. Mckenzie and H. Xu, *J. Am. Chem. Soc.*, 2003, **125**, 12384–12385.
57 D. Wang, F. Zhou, Y. Liu and W. Liu, *Mater. Lett.*, 2008, **62**, 1819–1822.
58 H. Imai, Y. Takei, K. Shimizu, M. Matsuda and H. Hirashima, *J. Mater. Chem.*, 1999, **9**, 2971–2972.
59 T. R. B. Foong, Y. Shen, X. Hu and A. Sellinger, *Adv. Funct. Mater.*, 2010, **20**, 1390–1396.
60 D. Wang, Y. Liu, B. Yu, F. Zhou and W. Liu, *Chem. Mater.*, 2009, **21**, 1198–1206.
61 Z. Su and W. Zhou, *J. Mater. Chem.*, 2009, **19**, 2301–2309.
62 K. Yasuda and P. Schmuki, *Electrochim. Acta*, 2007, **52**, 4053–4061.
63 A. Ghicov, H. Tsuchiya, J. M. Macak and P. Schmuki, *Electrochem. Commun.*, 2005, **7**, 505–509.
64 J. M. Macak, H. Tsuchiya, L. Taveira, S. Aldabergerova and P. Schmuki, *Angew. Chem., Int. Ed.*, 2005, **44**, 7463–7465.
65 C. Ruan, M. Paulose, O. K. Varghese, G. K. Mor and C. A. Grimes, *J. Phys. Chem. B*, 2005, **109**, 15754–15759.
66 M. Paulose, K. Shankar, S. Yoriya, H. E. Prakasam, O. K. Varghese, G. K. Mor, T. A. Latempa, A. Fitzgerald and C. A. Grimes, *J. Phys. Chem. B*, 2006, **110**, 16179–16184.
67 H. E. Prakasam, K. Shankar, O. K. M. PauloseVarghese and C. A. Grimes, *J. Phys. Chem. C*, 2007, **111**, 7235–7241.
68 M. Paulose, H. E. Prakasam, O. K. Varghese, L. Peng, K. C. Popat, G. K. Mor, T. A. Desai and C. A. Grimes, *J. Phys. Chem. C*, 2007, **111**, 14992–14997.
69 L. L. Li, C. Y. Tsai, H. P. Wu, C. C. Chen and E. W. G. Diau, *J. Mater. Chem.*, 2010, **20**, 2753–2758.
70 G. K. Mor, O. K. Varghese, M. Paulose and C. A. Grimes, *Adv. Funct. Mater.*, 2005, **15**, 1291–1296.
71 D. Wang and L. Liu, *Chem. Mater.*, 2010, **22**, 6656–6664.
72 C. Richter, Z. Wu, E. Panaitescu, R. J. Willey and L. Menon, *Adv. Mater.*, 2007, **19**, 946–948.
73 Q. A. Nguyen, Y. V. Bhargava and T. M. Devine, *Electrochem. Commun.*, 2008, **10**, 471–475.
74 N. K. Allam and C. A. Grimes, *J. Phys. Chem. C*, 2007, **111**, 13028–13032.
75 N. K. Allam, K. Shankar and C. A. Grimes, *J. Mater. Chem.*, 2008, **18**, 2341–2348.
76 K. S. Raja, T. Gandhi and M. Misra, *Electrochem. Commun.*, 2007, **9**, 1069–1076.
77 J. M. Macak and P. Schmuki, *Electrochim. Acta*, 2006, **52**, 1258–1264.
78 H. Tsuchiya, J. M. Macak, L. Taveira, E. Balaur, A. Ghicov, K. Sirotna and Patrik Schmuki, *Electrochem. Commun.*, 2005, **7**, 576–580.
79 S. Yoriya, M. Paulose, O. K. Varghese, G. K. Mor and C. A. Grimes, *J. Phys. Chem. C*, 2007, **111**, 13770–13776.
80 C. Ruan, M. Paulose, O. K. Varghese, G. K. Mor and C. A. Grimes, *J. Phys. Chem. B*, 2005, **109**, 15754–15759.
81 S. P. Albu, A. Ghicov, J. M. Macak, R. Hahn and P. Schmuki, *Nano Lett.*, 2007, **7**, 1286–1289.
82 K. Zhu, T. B. Vinzant, N. R. Neale and A. J. Frank, *Nano Lett.*, 2007, **7**, 3739–3746.
83 D. Wang, B. Yu, C. Wang, F. Zhou and W. Liu, *Adv. Mater.*, 2009, **21**, 1964–1967.
84 Z. Su and W. Zhou, *Adv. Mater.*, 2008, **20**, 3663–3667.
85 J. Wang and Z. Lin, *J. Phys. Chem. C*, 2009, **113**, 4026–4030.
86 G. K. Mor, K. Shankar, M. Paulose, O. K. Varghese and C. A. Grimes, *Nano Lett.*, 2006, **6**, 215–218.
87 J. H. Park, T. W. Lee and M. G. Kang, *Chem. Commun.*, 2008, 2867–2869.
88 Q. Chen and D. Xu, *J. Phys. Chem. C*, 2009, **113**, 6310–6314.
89 C. J. Lin, W. Y. Yu and S. H. Chien, *J. Mater. Chem.*, 2010, **20**, 1073–1077.
90 B. X. Lei, J. Y. Liao, R. Zhang, J. Wang, C. Y. Su and D. B. Kuang, *J. Phys. Chem. C*, 2010, **114**, 15228–15233.

91 J. Wang and Z. Lin, *Chem. Mater.*, 2008, **20**, 1257–1261.
92 O. K. Varghese, M. Paulose and C. A. Grimes, *Nat. Nanotechnol.*, 2009, **4**, 592–597.
93 J. Y. Li, C. Y. Chen, J. G. Chen, C. J. Tan, K. M. Lee, S. J. Wu, Y. L. Tung, H. H. Tsai, K. C. Ho and C. G. Wu, *J. Mater. Chem.*, 2010, **20**, 7158–7164.
94 G. Zhang, H. Bala, Y. Cheng, D. Shi, X. Lv, Q. Yu and P. Wang, *Chem. Commun.*, 2009, 2198–2200.
95 Y. Shengyuan, A. S. Nair, R. Jose and S. Ramakrishna, *Energy Environ. Sci.*, 2010, **3**, 2010–2014.
96 S. Q. Fan, D. Kim, J. J. Kim, D. W. Jung, S. O. Kang and J. Ko, *Electrochem. Commun.*, 2009, **11**, 1337–1339.
97 P. Xu, T. Xu, J. Lu, S. Gao, N. S. Hosmane, B. Huang, Y. Dai and Y. Wang, *Energy Environ. Sci.*, 2010, **3**, 1128–1134.
98 B. O'Regan and M. Grätzel, *Nature*, 1991, **353**, 737–740.
99 D. Kuang, P. Wang, S. Ito, S. M. Zakeeruddin and M. Grätzel, *J. Am. Chem. Soc.*, 2006, **128**, 7732–7733.
100 J. H. Yum, I. Jung, C. Baik, J. Ko, M. K. Nazeeruddin and M. Grätzel, *Energy Environ. Sci.*, 2009, **2**, 100–102.
101 D. Kuang, S. Ito, B. Wenger, C. Klein, J. E. Moser, R. Humphry-Baker, S. M. Zakeeruddin and M. Grätzel, *J. Am. Chem. Soc.*, 2006, **128**, 4146–4154.
102 H. Qin, S. Wenger, M. Xu, F. Gao, X. Jing, P. Wang, S. M. Zakeeruddin and M. Grätzel, *J. Am. Chem. Soc.*, 2008, **130**, 9202–9203.
103 H. Choi, C. Baik, S. O. Kang, J. Ko, M. S. Kang, M. K. Nazeeruddin and M. Grätzel, *Angew. Chem., Int. Ed.*, 2008, **47**, 327–330.
104 C. Y. Chen, J. G. Chen, S. J. Wu, J. Y. Li, C. G. Wu and K. C. Ho, *Angew. Chem., Int. Ed.*, 2008, **47**, 7342–7345.
105 P. Wang, S. M. Zakeeruddin, J. E. Moser, R. Humphry-Baker and M. Grätzel, *J. Am. Chem. Soc.*, 2004, **126**, 7164–7165.
106 M. K. Nazeeruddin, F. D. Angelis, S. Fantacci, A. Selloni, G. Viscardi, P. Liska, S. Ito, B. Takeru and M. Grätzel, *J. Am. Chem. Soc.*, 2005, **127**, 16835–16847.
107 A. Mishra, M. K. R. Fischer and P. Bäuerle, *Angew. Chem., Int. Ed.*, 2009, **48**, 2474–2499.
108 F. Gao, Y. Wang, D. Shi, J. Zhang, M. Wang, X. Jing, R. Humphry-Baker, P. Wang, S. M. Zakeeruddin and M. Grätzel, *J. Am. Chem. Soc.*, 2008, **130**, 10720–10728.
109 F. Gao, Y. Wang, J. Zhang, D. Shi, M. Wang, R. Humphry-Baker, P. Wang, S. M. Zakeeruddin and M. Grätzel, *Chem. Commun.*, 2008, 2635–2637.
110 J. Y. Li, C. Y. Chen, J. G. Chen, C. J. Tan, K. M. Lee, S. J. Wu, Y. L. Tung, H. H. Tsai, K. C. Ho and C. G. Wu, *J. Mater. Chem.*, 2010, **20**, 7158–7164.
111 S. L. Wu, H. P. Lu, H. T. Yu, S. H. Chuang, C. L. Chiu, C. W. Lee, E. W. G. Diau and C. Y. Yeh, *Energy Environ. Sci.*, 2010, **3**, 949–955.
112 Y. Kim, C. H. Kim, Y. Lee and K. J. Kim, *Chem. Mater.*, 2010, **22**, 207–211.
113 N. Yang, J. Zhai, D. Wang, Y. Chen and L. Jiang, *ACS Nano*, 2010, **4**, 887–894.
114 J. M. Macák, H. Tsuchiya, A. Ghicov and P. Schmuki, *Electrochem. Commun.*, 2005, **7**, 1133–1137.
115 D. Kim, A. Ghicov and P. Schmuki, *Electrochem. Commun.*, 2008, **10**, 1835–1838.
116 J. R. Jennings, A. Ghicov, L. M. Peter, P. Schmuki and A. B. Walker, *J. Am. Chem. Soc.*, 2008, **130**, 13364–13372.
117 A. Ghicov, S. P. Albu, R. Hahn, D. Kim, T. Stergiopoulos, J. Kunze, C. A. Schiller, P. Falaras and P. Schmuki, *Chem.–Asian J.*, 2009, **4**, 520–525.
118 C. H. Chen, Y. C. Hsu, H. H. Chou, K. R. Justin Thomas, J. T. Lin and C. P. Hsu, *Chem.–Eur. J.*, 2010, **16**, 3184–3193.
119 M. Wang, S. J. Moon, M. Xu, K. Chittibabu, P. Wang, N. L. Cevey-Ha, R. Humphry-Baker, S. M. Zakeeruddin and M. Grätzel, *Small*, 2010, **6**, 319–324.
120 Y. Xie, G. Ali, S. H. Yoo and S. O. Cho, *ACS Appl. Mater. Interfaces*, 2010, **2**, 2910–2914.
121 H. Lee, M. Wang, P. Chen, D. R. Gamelin, S. M. Zakeeruddin, M. Grätzel and M. K. Nazeeruddin, *Nano Lett.*, 2009, **9**, 4221–4227.
122 M. Grätzel, *Nature*, 2001, **414**, 338–344.
123 A. Kongkanand, K. Tvrdy, K. Takechi, M. Kuno and P. V. Kamat, *J. Am. Chem. Soc.*, 2008, **130**, 4007–4015.
124 D. Wang, H. Zhao, N. Wu, M. A. E. Khakani and D. Ma, *J. Phys. Chem. Lett.*, 2010, **1**, 1030–1035.
125 R. Plass, S. Pelet, J. Krueger and M. Grätzel, *J. Phys. Chem. B*, 2002, **106**, 7578–7580.
126 L. M. Peter, K. G. U. Wijayantha, D. J. Riley and J. P. Waggett, *J. Phys. Chem. B*, 2003, **107**, 8378–8381.
127 P. Yu, K. Zhu, A. G. Norman, S. Ferrere, A. J. Frank and A. J. Nozik, *J. Phys. Chem. B*, 2006, **110**, 25451–25454.
128 S. K. Sarkar, J. Y. Kim, D. N. Goldstein, N. R. Neale, K. Zhu, C. M. Elliott, A. J. Frank and S. M. George, *J. Phys. Chem. C*, 2010, **114**, 8032–8039.
129 T. L. Li and H. Teng, *J. Mater. Chem.*, 2010, **20**, 3656–3664.
130 E. M. Barea, M. Shalom, S. Giménez, I. Hod, I. Mora-Seró, A. Zaban and J. Bisquert, *J. Am. Chem. Soc.*, 2010, **132**, 6834–6839.
131 W. T. Sun, Y. Yu, H. Y. Pan, X. F. Gao, Q. Chen and L. M. Peng, *J. Am. Chem. Soc.*, 2008, **130**, 1124–1125.
132 D. R. Baker and P. V. Kamat, *Adv. Funct. Mater.*, 2009, **19**, 805–811.
133 S. Chen, M. Paulose, C. Ruan, G. K. Mor, O. K. Varghese, D. Kouzoudis and C. A. Grimes, *J. Photochem. Photobiol., A*, 2006, **177**, 177–184.
134 X. F. Gao, W. T. Sun, Z. D. Hu, G. Ai, Y. L. Zhang, S. Feng, F. Li and L. M. Peng, *J. Phys. Chem. C*, 2009, **113**, 20481–20485.
135 C. Ratanatawanate, C. Xiong and K. J. B. Jr, *ACS Nano*, 2008, **2**, 1682–1688.
136 X. F. Gao, H. B. Li, W. T. Sun, Q. Chen, F. Q. Tang and L. M. Peng, *J. Phys. Chem. C*, 2009, **113**, 7531–7535.
137 K. Shin, S. i. S, S. H. Im and J. H. Park, *Chem. Commun.*, 2010, **46**, 2385–2387.
138 W. Zhu, X. Liu, H. Liu, D. Tong, J. Yang and J. Peng, *J. Am. Chem. Soc.*, 2010, **132**, 12619–12626.
139 M. Shalom, S. Dor, S. Rühle, L. Grinis and A. Zaban, *J. Phys. Chem. C*, 2009, **113**, 3895–3898.
140 I. Mora-Seró, S. Giménez, F. Fabregat-Santiago, R. Gómez, Q. Shen, T. Toyoda and J. Bisquert, *Acc. Chem. Res.*, 2009, **42**, 1848–1857.
141 Y. L. Lee and Y. S. Lo, *Adv. Funct. Mater.*, 2009, **19**, 604–609.
142 S. Yang, C. Huang, J. Zhai, Z. Wang and L. Jiang, *J. Mater. Chem.*, 2002, **12**, 1459–1464.
143 H. Lee, H. C. Leventis, S. J. Moon, P. Chen, S. Ito, S. A. Haque, T. Torres, F. Nüesch, T. Geiger, S. M. Zakeeruddin, M. Grätzel and M. K. Nazeeruddin, *Adv. Funct. Mater.*, 2009, **19**, 2735–2742.
144 H. C. Leventis and S. A. Haque, *Energy Environ. Sci.*, 2009, **2**, 1176–1179.
145 M. Shalom, J. Albero, Z. Tachan, E. Martínez-Ferrero, A. Zaban and E. Palomares, *J. Phys. Chem. Lett.*, 2010, **1**, 1134–1138.
146 A. Ghicov, J. M. Macak, H. Tsuchiya, J. Kunze, V. Haeublein, L. Frey and P. Schmuki, *Nano Lett.*, 2006, **6**, 1080–1082.
147 J. H. Park, S. Kim and A. J. Bard, *Nano Lett.*, 2006, **6**, 24–28.
148 S. Bingham and W. A. Daoud, *J. Mater. Chem.*, 2011, **21**, 2041–2050.
149 J. He, Q. Liu, Z. Sun, W. Yan, G. Zhang, Z. Qi, P. Xu, Z. Wu and S. Wei, *J. Phys. Chem. C*, 2010, **114**, 6035–6038.
150 X. L., X. Mou, J. Wu, D. Zhang, L. Zhang, F. Huang, F. Xu and S. Huang, *Adv. Funct. Mater.*, 2010, **20**, 509–515.
151 H. J. Park, M. G. Kang, S. H. Ahn and L. J. Guo, *Adv. Mater.*, 2010, **22**, E247–E253.
152 S. S. v. Bavel, M. Bärenklau, G. d. With, H. Hoppe and J. Loos, *Adv. Funct. Mater.*, 2010, **20**, 1458–1463.
153 T. Ameri, G. Dennler, C. Waldauf, H. Azimi, A. Seemann, K. Forberich, J. Hauch, M. Scharber, K. Hingerl and C. J. Brabec, *Adv. Funct. Mater.*, 2010, **20**, 1592–1598.
154 B. C. Thompson and J. M. J. Fréchet, *Angew. Chem., Int. Ed.*, 2008, **47**, 58–77.
155 G. Yu, J. Gao, J. C. Hummelen, F. Wudl and A. J. Heeger, *Science*, 1995, **270**, 1789–1791.
156 M. Koppe, H. J. Egelhaaf, G. Dennler, M. C. Scharber, C. J. Brabec, P. Schilinsky and C. N. Hoth, *Adv. Funct. Mater.*, 2010, **20**, 338–346.
157 R. Po, M. Maggini and N. Camaioni, *J. Phys. Chem. C*, 2010, **114**, 695–706.
158 Y. He, H. Y. Chen, J. Hou and Y. Li, *J. Am. Chem. Soc.*, 2010, **132**, 1377–1382.
159 M. Shin, H. Kim, J. Park, S. Nam, K. Heo, M. Ree, C. S. Ha and Y. Kim, *Adv. Funct. Mater.*, 2010, **20**, 748–754.
160 W. Ma, C. Yang, X. Gong, K. Lee and A. J. Heeger, *Adv. Funct. Mater.*, 2005, **15**, 1617–1622.
161 Y. Liang, D. Feng, Y. Wu, S. T. Tsai, G. Li, C. Ray and L. Yu, *J. Am. Chem. Soc.*, 2009, **131**, 7792–7799.

162 J. S. Kim, Y. Lee, J. H. Lee, J. H. Park, J. K. Kim and K. Cho, *Adv. Mater.*, 2010, **22**, 1355–1360.
163 S. Sista, Z. Hong, M. H. Park, Z. Xu and Y. Yang, *Adv. Mater.*, 2010, **22**, E77–E80.
164 J. Gilot, M. M. Wienk and R. A. J. Janssen, *Adv. Mater.*, 2010, **22**, E67–E71.
165 J. Y. Kim, K. Lee, N. E. Coates, D. Moses, T. Q. Nguyen, M. Dante and A. J. Heeger, *Science*, 2007, **317**, 222–225.
166 K. Shankar, G. K. Mor, H. E. Prakasam, O. K. Varghese and C. A. Grimes, *Langmuir*, 2007, **23**, 12445–12449.
167 Y. Y. Lin, T. H. Chu, S. S. Li, C. H. Chuang, C. H. Chang, W. F. Su, C. P. Chang, M. W. Chu and C. W. Chen, *J. Am. Chem. Soc.*, 2009, **131**, 3644–3649.
168 R. Zhu, C. Y. Jiang, B. Liu and S. Ramakrishna, *Adv. Mater.*, 2009, **21**, 994–1000.
169 S. Tepavcevic, S. B. Darling, N. M. Dimitrijevic, T. Rajh and S. J. Sibener, *Small*, 2009, **5**, 1776–1783.
170 M. D. Lua and S. M. Yang, *J. Colloid Interface Sci.*, 2009, **333**, 128–134.
171 Y. Zhang, C. Wang, L. Rothberg and M. K. Ng, *J. Mater. Chem.*, 2006, **16**, 3721–3725.
172 V. Senkovskyy, R. Tkachov, T. Beryozkina, H. Komber, U. Oertel, M. Horecha, V. Bocharova, M. Stamm, S. A. Gevorgyan, F. C. Krebs and A. Kiriy, *J. Am. Chem. Soc.*, 2009, **131**, 16445–16453.
173 D. Wang, Q. Ye, B. Yu and F. Zhou, *J. Mater. Chem.*, 2010, **20**, 6910–6915.
174 P. Roy, D. Kim, I. Paramasivam and P. Schmuki, *Electrochem. Commun.*, 2009, **11**, 1001–1004.
175 J. G. Chen, C. Y. Chen, C. G. Wu, C. Y. Lin, Y. H. Lai, C. C. Wang, H. W. Chen, R. Vittal and K. C. Ho, *J. Mater. Chem.*, 2010, **20**, 7201–7207.
176 J. Wang and Z. Lin, *Chem. Mater.*, 2010, **22**, 579–584.
177 D. Wang, T. Hu, L. Hu, B. Yu, Y. Xia, F. Zhou and W. Liu, *Adv. Funct. Mater.*, 2009, **19**, 1930–1938.
178 D. Kim, K. Lee, P. Roy, B. I. Birajdar, E. Spiecker and P. Schmuki, *Angew. Chem., Int. Ed.*, 2009, **48**, 9326–9329.
179 K. Lee, D. Kim, P. Roy, I. Paramasivam, B. I. Birajdar, E. Spiecker and P. Schmuki, *J. Am. Chem. Soc.*, 2010, **132**, 1478–1479.
180 D. Kim, A. Ghicov, S. P. Albu and P. Schmuki, *J. Am. Chem. Soc.*, 2008, **130**, 16454–16455.
181 D. Wang, X. Wang, X. Liu and F. Zhou, *J. Phys. Chem. C*, 2010, **114**, 9938–9944.
182 J. Wang, L. Zhao, V. S.-Y. Lin and Z. Lin, *J. Mater. Chem.*, 2009, **19**, 3682–3687.
183 K. Zhu, N. R. Neale, A. F. Halverson, J. Y. Kim and A. J. Frank, *J. Phys. Chem. C*, 2010, **114**, 13433–13441.
184 X. Fang, T. l. Ma, M. Akiyama, G. Guan, S. Tsunematsu and E. Abe, *Thin Solid Films*, 2005, **472**, 242–245.
185 M. G. Kang, N. G. Park, K. S. Ryu, S. H. Chang and K. J. Kim, *Sol. Energy Mater. Sol. Cells*, 2006, **90**, 574–581.
186 S. Ito, N. L. C. Ha, G. Rothenberger, P. Liska, P. Comte, S. M. Zakeeruddin, P. Péchy, M. K. Nazeeruddin and M. Grätzel, *Chem. Commun.*, 2006, 4004–4006.
187 W. Tan, X. Yin, X. Zhou, J. Zhang, X. Xiao and Y. Lin, *Electrochim. Acta*, 2009, **54**, 4467–4472.
188 Q. Wang, K. Zhu, N. R. Neale and A. J. Frank, *Nano Lett.*, 2009, **9**, 806–813.
189 G. Zhang, H. Huang, Y. Zhang, H. L. W. Chan and L. Zhou, *Electrochem. Commun.*, 2007, **9**, 2854–2858.
190 Y. Shin and S. Lee, *Nano Lett.*, 2008, **8**, 3171–3173.
191 D. Wang, Y. Liu, C. Wang, F. Zhou and W. Liu, *ACS Nano*, 2009, **3**, 1249–1257.